Nanoscience and Nanotechnology 2014, 4(1): 7-15
DOI: 10.5923/j.nn.20140401.02

Spherical Nanoparticles of Eu^{3+}-doped ZnS Semiconductor Synthesized from ZnO Nanorods Precursor

Ahemen I.[1,*], Amah A. N.[1], AttahDaniel B. E.[2], Fasasi A. Y.[3]

[1]Department of Physics, University of Agriculture, Makurdi, 97001, Nigeria
[2]Research & Development Department, Engineering Materials Development Institute, Akure, Nigeria
[3]DCenter for Energy Research Development, Obafemi Awolowo University, Ile-Ife, Nigeria

Abstract In this paper, synthesis of europium doped-zinc sulfide (Eu^{3+}: ZnS) spherical nanoparticles was carried out using freshly prepared zinc oxide (ZnO) nanorods precursor. The synthetic method used was the precipitation technique. Both ZnO nanorods and Eu^{3+}: ZnS spherical nanoparticles were characterized by X-ray diffraction (XRD) analyses, transmission electron microscopy (TEM), scanning electron microscopy (SEM), UV-Visible spectroscopy and photoluminescence studies. XRD results indicate crystalline nanoparticles with zinc blende and wurzite structures for Eu^{3+}: ZnS spherical nanoparticles and ZnO nanorods, respectively. The lattice strain ($13.81x10^{-3}$ for Eu^{3+}: ZnS and $3.98x10^{-3}$ for ZnO) shows that Eu^{3+}: ZnS spherical nanoparticles have a ten-fold increase in deformation which is likely caused by the introduction of Eu^{3+} into the ZnS matrix. The morphology of the spherical nanoparticles and nanorods were confirmed from SEM and TEM results. Photoluminescence emission studies revealed that no energy transfer between Eu^{3+} ion and host ZnS took place. UV-Visible spectroscopic studies show considerable blue-shift in the absorption energy for both ZnO nanorods (277 nm) and Eu^{3+}: ZnS spherical nanoparticles (300 nm).

Keywords Europium, Zinc sulfide, Spherical nanoparticles, Nanorods, Doped, Strain

1. Introduction

Nanophosphors have promising potentials to supplant or replace conventional microcrystalline phosphors in optoelectronic devices due to the advantage of changing the luminescent properties of nanophosphors with reduced dimensions. The emission lifetime and rich spectral properties of europium ion has made it attractive in different applications such as flat panel displays (FPD), plasma display panel (PDP), cathode-ray tubes (CRT), fluorescent lamps and light emitting diodes etc. However, because of low small absorption coefficient, only limited amount of radiation can be absorbed by direct excitation in the 4f levels of Eu^{3+} ion[1]. Since luminescence intensity is proportional to both luminescence quantum yield and the amount of light absorbed, weak light absorption will result in weak luminescence. Therefore, Eu^{3+} ion requires the use of suitable host materials to excite (sensitize) the Eu^{3+} ion efficiently in a wide spectral range. Because for Eu^{3+} ion the4f level is shielded from the effect of host crystal field, the f –f transition is forbidden under the Laport rule. Therefore, a suitable host must be capable of providing low site symmetry for the ion in order to relax the Laport rule. Among the host materials used for Eu^{3+} ions are TiO_2[2], $Y_3Al_5O_{12}$[3], In_2S_3[4], SnO_2[5], GaN[6], SiO_2[7], CdS[8], ZnO[9] and ZnS[10] etc.

ZnS doped europium have been reported by many authors, however, energy transfer from ZnS host to Eu^{3+} ion center is in doubt. This is because of the low phonon energy of ZnS and the energy mismatch between the ZnS host and the Eu^{3+} ion center[11]. In comparison with ZnS host, energy transfer from excited ZnO host to Eu^{3+} have been shown to be more favourable because of the available matching levels[9]. Also, there is a controversy on whether Eu^{3+} can be incorporated into ZnS semiconductor lattice giving the large differences in ionic radii and charge imbalance[8]. Some reports have suggested that incorporating Eu^{3+} into ZnS matrix could be possible if the synthetic method is well-designed and the charge imbalance is compensated[7, 11]. In this regard, synthetic routes such as sol-gel[10], arrested precipitation [12] and microemulsion[13] have been employed to dope ZnS nanoparticles with Eu^{3+} ion.

Nanophosphors of spherical morphology, narrow size distribution and low dispersity are desired to improve the emission intensity and screen packing[2, 14]. Spherical

* Corresponding author:
ahemen.iorkyaa@uam.edu.ng (Ahemen I.)
Published online at http://journal.sapub.org/nn

morphology of phosphor is also good for high brightness, high resolution and low scattering of light[15, 16, 17]. In this work, we study the possibility of incorporating Eu^{3+} ion into spherical ZnS nanoparticles, their energy transfer prospect and enhancement of luminescent emission intensity through a new synthetic route. This synthetic route involves first synthesizing ZnO nanorods and then converting the rods to spherical ZnS nanophosphors after doping with Eu^{3+} ion.

2. Experiment

The synthesis of ZnS: Eu^{3+} nanophosphor was carried out in two stages; firstly ZnO nanoparticles were synthesized and secondly a portion of the ZnO nanoparticles was used as a precursor for the preparation of ZnS: Eu^{3+} nanophosphor. All reagents used in this work are of analytical grade and were used as received without further purification.

2.1. Synthesis of ZnO Nanorods

ZnO nanoparticles were synthesized at room temperature using arrested precipitation technique. 10g of NaOH was made into solution and was drop-wise added to a solution containing 53.76g of zinc acetate while stirring. The mixture was stirred to obtain white precipitate which was then centrifuge at 3500 revolutions per minutes (rpm) for 20 min. This was followed by washing the precipitates in ethanol and de-ionized water. The precipitate was dried for 10 hours at 80℃ to obtain a white solid which was made into fine powder by grinding.

The reaction equation for the formation of ZnO is as follows;

$$Zn(CH_3COO)_2 + 2NaOH \rightarrow 2CH_3COONa + Zn(OH)_2 \quad (1)$$

$$Zn^{2+} + 2OH^- + Zn(OH)_2 \quad (2)$$

$$Zn(OH)_2 \xrightarrow{Heat} ZnO + H_2O \uparrow \quad (3)$$

2.2. Synthesis of Spherical ZnS:Eu^{3+} Nanoparticles

The co-precipitation method was used to synthesize spherical ZnS: Eu^{3+} nanoparticles. 3.033g of the freshly prepared ZnO powder was mixed with 0.916g of $EuCl_3$ (representing 5mol% doping concentration) and dried. 100 ml binary solution of ethanol-deionized water added to the mixture and refluxed at 80℃ for 1hour. Meanwhile, 11.269g of thioacetamide (TAA) was separately dissolved in 150 ml of ethanol-water binary solution and also heated for 1 hour. Both solutions were allowed to cool at room temperature before mixing. Alpha-methacrylic acid was added to the mixture and the pH was adjusted to a value of 3 using acetic acid. The obtained white precipitate was centrifuged at 3500 rpm for 20 min, followed by washing several times with ethanol and then drying at 80℃ for 12 hours. Finally, the obtained solid was made into fine powder by grinding. The precipitate was dried for 10 hours at 80℃ to obtain a white solid which was made into fine powder by grinding.

The reaction equation for the formation of ZnS:Eu^{3+} is as follows;

$$CH_3CSNH_2 + H_2O \rightarrow CH_3(NH_2)C(OH) - SH \quad (4)$$

$$CH_3(NH_2)C(OH)SH + H_2O \rightarrow CH_3(NH_2)C(OH)_2 + H_2S \quad (5)$$

$$CH_3(NH_2)C(OH)_2 \rightarrow H_2O + CH_3(NH_2)C = O \quad (6)$$

$$EuCl_3 \xrightarrow{H_2O} Eu^{3+} + 3Cl^- \quad (7)$$

Combining equations (3), (5) and (7), gives;

$$Zn^{2+} + Eu^{3+} + S^{2-} \rightarrow ZnS : Eu^{3+} \quad (8)$$

2.3. Characterization

Structural characteristics of obtained ZnO and ZnS: Eu^{3+} powder were explored by X-ray diffraction method using PANalytical XPERT-PRO diffraction machine with CuK_α radiation ($\lambda = 1.5406\,\text{Å}$) with 2θ ranging between 10^o and 90^o. Transmission electron microscopy (TEM) studies of samples were carried out using JEOL-JEM 2100 Transmission Microscope. Ultraviolet-visible absorption spectrum was obtained from JENWAY 6405 spectrophotometer. The shape and size of the particles were estimated by scanning electron microscopy (JEOL-JSM 7500F), while the elemental mapping of Eu in the ZnS was carried out using energy dispersive spectroscope attached to the SEM. Photoluminescence spectra of ZnO and Eu-doped ZnS samples were recorded with Perkin-Elmer LS-55 Fluorescence spectrometer. All measurements were carried out at room temperature under ambient atmosphere.

2.4. Crystallite Size and Strain Determination

The Debye-Scherrer equation for estimating crystallite size from XRD pattern is given by:

$$D = \frac{K\lambda}{\beta \cos\theta} \quad (9)$$

where λ is the wavelength of CuK_α radiation ($\lambda = 1.54056\,\text{Å}$), D is the crystallite size, K is a constant (K= 0.9), θ is the diffraction peak position and β_D is the broadening solely due to small crystallite size. The Scherrer equation assumes peak broadening of the diffraction breadth to be solely the effect of crystallite size. However, it is established that peak broadening could also be caused by other factors such as instrumental broadening (β_i) and broadening due to lattice strain (β_s). The observed peak broadening (β_o) in Fig. 1 can therefore be expressed by:

$$\beta_o = \beta_i + \beta_{hkl} \quad (10)$$

where $\beta_{hkl} = \beta_S + \beta_D$ is the broadening due to crystallite size and strain. The instrumental broadening was obtained from a coarse-grained, well-annealed high purity silver powder (standard) sample subjected to XRD under identical conditions as those for the test samples. Equation (10) holds if the diffraction peaks are purely Cauchy profile. However, the diffraction peaks in Fig. 1 shows better fits to the pseudo-voigt profile. The integral breadth width due to this broadening effect of the X-ray diffraction peak is given by[18]:

$$\beta_{hkl} = [(\beta_o - \beta_i)(\beta_o^2 - \beta_i^2)] \quad (11)$$

The broadening due to lattice strain (ε) can be estimated from Stokes-Wilson equation given by[19]:

$$\beta_s = 4\varepsilon \tan\theta \quad (12)$$

The dislocation densities (δ) of ZnS and ZnO are expressed by $(\delta = 15\varepsilon/aD)$ and $(\delta = 1/D^2)$, respectively [15, 19, 20] where a is the lattice parameter in a cubic structure given as;

$$a = d_{hkl}(h^2 + k^2 + l^2)^{1/2} \quad (13)$$

with the unit cell volume as $V_{ZnS} = a^3$, and for a wurzite structure we have;

$$a = \left[\frac{4}{3}(h^2 + hk + l^2)\left(\frac{1}{d_{hkl}^2} - \frac{l^2}{c^2}\right)^{-1}\right]^{1/2} \quad (14)$$

with a unit cell volume given by $V_{ZnO} = \frac{\sqrt{3}a^2c}{2}$.

For a uniformly strained crystal, Williamson-Hall (W-H) expressed the peak broadening as a linear combination from crystallite size (equation 9) and crystal imperfections/ distortion (lattice strain, ε) (equation 12)[21]:

$$\beta_{hkl}\cos\theta = \left(\frac{K\lambda}{D}\right) + (4\varepsilon\sin\theta) \quad (15)$$

The plot of $\beta_{hkl}\cos\theta$ versus $4\sin\theta$ from equation (15) gives a straight line with the slope equal to the strain, (ε) and the intercept along the $\beta_{hkl}\cos\theta$ axis equal $K\lambda/D$ from where the crystallite size can be calculated.

3. Results and Discussion

3.1. Crystallite Structure, Size and Strain

The XRD patterns of ZnO nanorods and Eu^{3+}-doped ZnS spherical nanoparticles shown in Fig. 1 have evident peaks which could be indexed to ZnO wurzite structure (JCPDS No. 31-1451) and cubic (zinc blende) structure of ZnS (JCPDS No. 05-0566). No other impurity signals attributed to free reactants or other compounds such as Eu_2O_3 was found in the XRD patterns which is an indication that Eu^{3+} ions are well dispersed inside the host matrix without cluster formation. The average crystallite sizes estimated from the XRD peak widths using the Scherrer equation (equation 9) are 25.5 nm and 2.9 nm for ZnO and Eu^{3+}: ZnS powders respectively. Similarly, the estimated crystallite sizes using the Williamson-Halls equation (equation 15) for ZnO and Eu^{3+}: ZnS powders are 36.2 nm and 4.1 nm, respectively. The larger crystallite sizes obtained using W-H plots (Fig. 2 and Fig. 3) is more accurate because the Scherrer equation does not take into consideration the effect of lattice strain in the line broadening[22]. The implication is that, the Scherrer equation overestimates the effect of crystallite size[13].

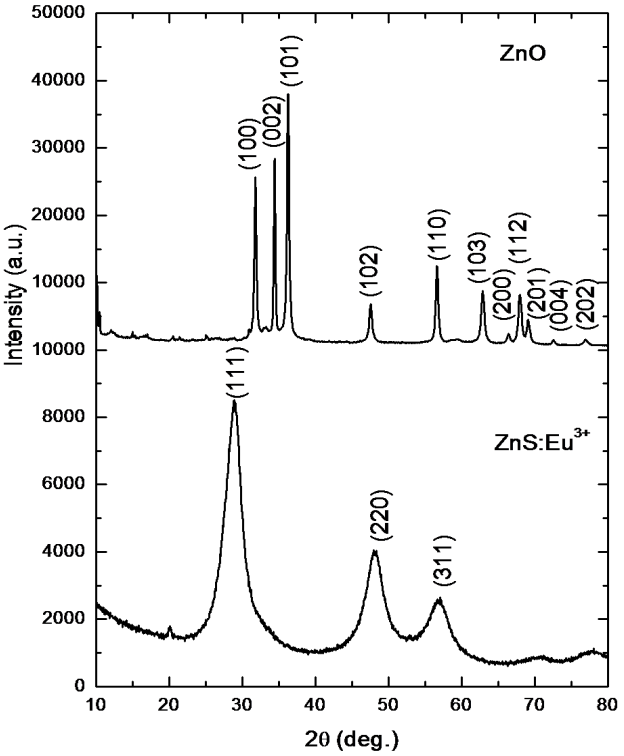

Figure 1. X-Ray Diffraction patterns of ZnO nanorods and Eu^{3+}: ZnS spherical nanoparticles

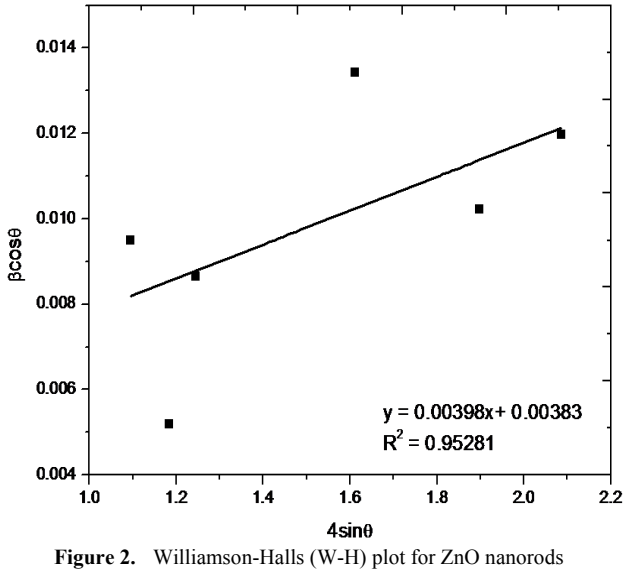

Figure 2. Williamson-Halls (W-H) plot for ZnO nanorods

Table 1. The Structural and Geometrical Parameters of ZnO Nanorods and ZnS: Eu^{3+} Nanoparticles

Sample	Scherrer's method D(nm)	W-H method D(nm)	TEM D(nm)	SEM D (nm)	Lattice Parameters ^{o}(A)	Cell Volume $^{o}(A^3)$	Strain $\varepsilon \times 10^{-3}$	$\delta \times 10^{-4}$ (Lines/m^2)
ZnO	25.5	36.2	11.6	25.6×8.6	$a = 3.2515$ $c = 5.4625$	50.01	3.98	7.63
Eu^{3+}: ZnS	2.9	4.1	2.8	10.7	$a = 5.5110$	167.38	13.81	91.7

From the W-H plots in Fig. 2 and Fig. 3, the lattice distortion ratio (strain, e) of 3.98×10^{-3} and 13.81×10^{-3} was obtained for ZnO nanorods and Eu^{3+}: ZnS spherical nanoparticles, respectively. Their respective dislocation densities are given in Table 1. The larger lattice strain and dislocation density obtained for Eu^{3+}: ZnS spherical nanoparticles could be associated with the introduction of small quantity of Eu^{3+} ion in the crystal lattice of ZnS. Europium (III) ion has a much larger ionic radius $r(Eu^{3+}) = 0.095nm$ than Zn^{2+} ion $r(Zn^{2+}) = 0.075nm$ [24]. Therefore, substitution of Eu^{3+} into Zn^{2+} lattice site would lead to a much higher distortion of the periodic lattice of the host. This argument can be collaborated by the large lattice constant and unit cell volume of Eu^{3+}: ZnS nanoparticles when compared with the standard value and other reports on ZnS[25; JCPDS No. 31-1451].

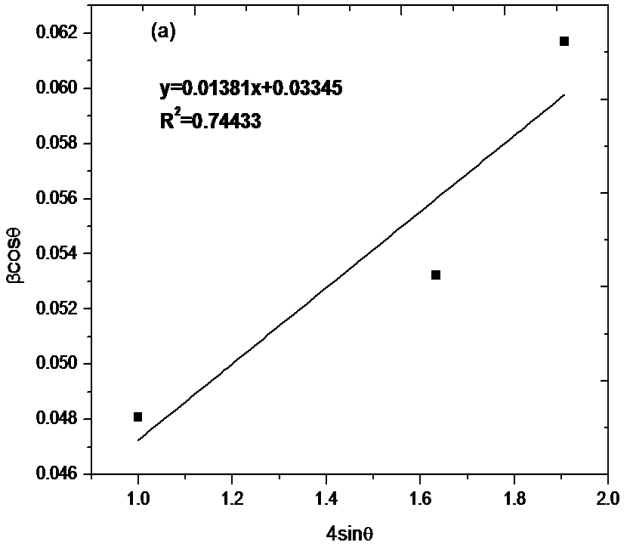

Figure 3. Williamson-Halls plot for Eu^{3+}: ZnS spherical nanoparticles

3.2. Morphology

Figure 4 displays the TEM and HRTEM images of ZnO nanorods and Eu^{3+}: ZnS nanoparticles. The average crystal sizes determined from which figure 4 (a) and (b) are 11.6 nm and 2.8 nm for ZnO nanorods and Eu^{3+}: ZnS nanoparticles, respectively. These values are in close agreement with the results obtained from powdered XRD analysis of the samples using Scherrer's formula for Eu: ZnS nanoparticles. The interference fringes of the (101) and (111) planes of some particles can be clearly observed from the HRTEM images shown in Fig.4(c) and 4(d). The lattice spacing values of 0.3182 nm and 0.2731 nm measured from these images for ZnO nanorods and Eu^{3+}: ZnS nanoparticles, respectively agree fairly well with standard values.

In Fig. 5(a) is shown the SEM micrographs of of ZnO nanorods. The micrograph contains large quantities of segmented nanorods with average length of 25.6 nm and diameter of 8.6 nm. Fig. 5(b) is the SEM image of clustered of Eu^{3+}: ZnS spherical nanoparticles with average size of 10.7 nm. The variation in particle sizes shown in Table 1 may be due to the inclusion of agglomerates in size measurement (e.g. SEM) or overestimation from the scattered point distribution obtained in the W-H technique. The mechanism of conversion of ZnO nanorods to spherical ZnS nanoparticles can be explained as follows; a gradual release of S^{2-} ion after the addition of TAA in the solution and the presence of NH_2^- may be responsible for the structural conversion from rods to spherical particles. During the conversion process, ion exchange between H_2S and ZnO occur in the solution mixture. The S^{2-} reacted with Zn^{2+} slowly forming ZnS shell on the ZnO surface under the driving force caused by the fact that ZnS is more thermodynamically stable due to lower solubility product (K_{SP}) (i.e. $K_{SP} = 6.8 \times 10^{-17}$ for ZnO and $K_{SP} = 1.2 \times 10^{-24}$ for ZnS). As a result of continuous diffusion of Zn^{2+} from inside of ZnO cores to the outer surface of the ZnS shell along certain ZnO bridges[26] to react with S^{2-} in solution, ZnS shell will continue to grow thicker while the ZnO core grows thinner. For the smaller-size nanorods obtained in our case, it is possible that all the ZnO rods are consumed into ZnS formation. Energy dispersive spectroscopy (EDS) analysis of the synthesized samples in Fig. 5(c) and (d) showed the pure form of ZnO nanorod and spherical nanoparticles of ZnS doped with Eu^{3+} ion. No sulfur and europium were present in the EDS spectrum of ZnO powdered sample (Fig. 5c). Similarly, for Eu^{3+}: ZnS sample spectrum (Fig. 5d); only Zn, Eu and S were observed indicating the formation of the pure substance. In Fig. 5d, the relatively very weak oxygen peak (when compared to Fig. 5c) between 0 and 1 keV could be from air trapped in the SEM chamber.

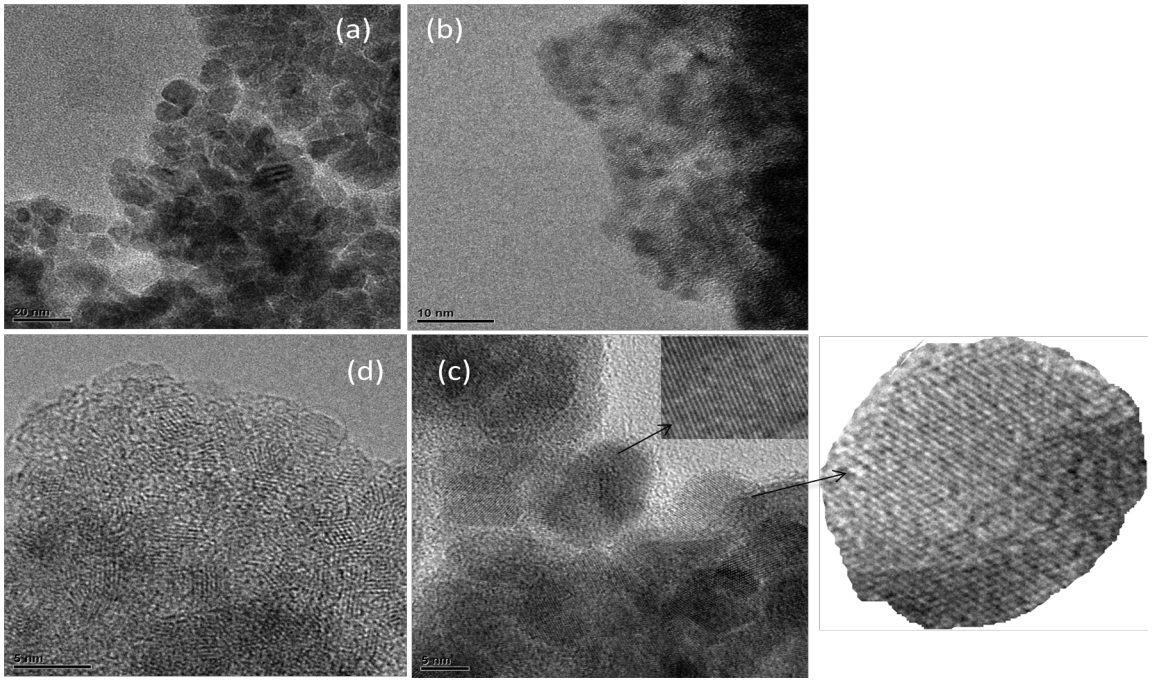

Figure 4. (a) TEM image of ZnO nanorods, (b)TEM image of Eu^{3+}: ZnS spherical nanoparticles, (c) HRTEM image of ZnO nanorods and (d) HRTEM image of Eu^{3+}: ZnS spherical nanoparticles

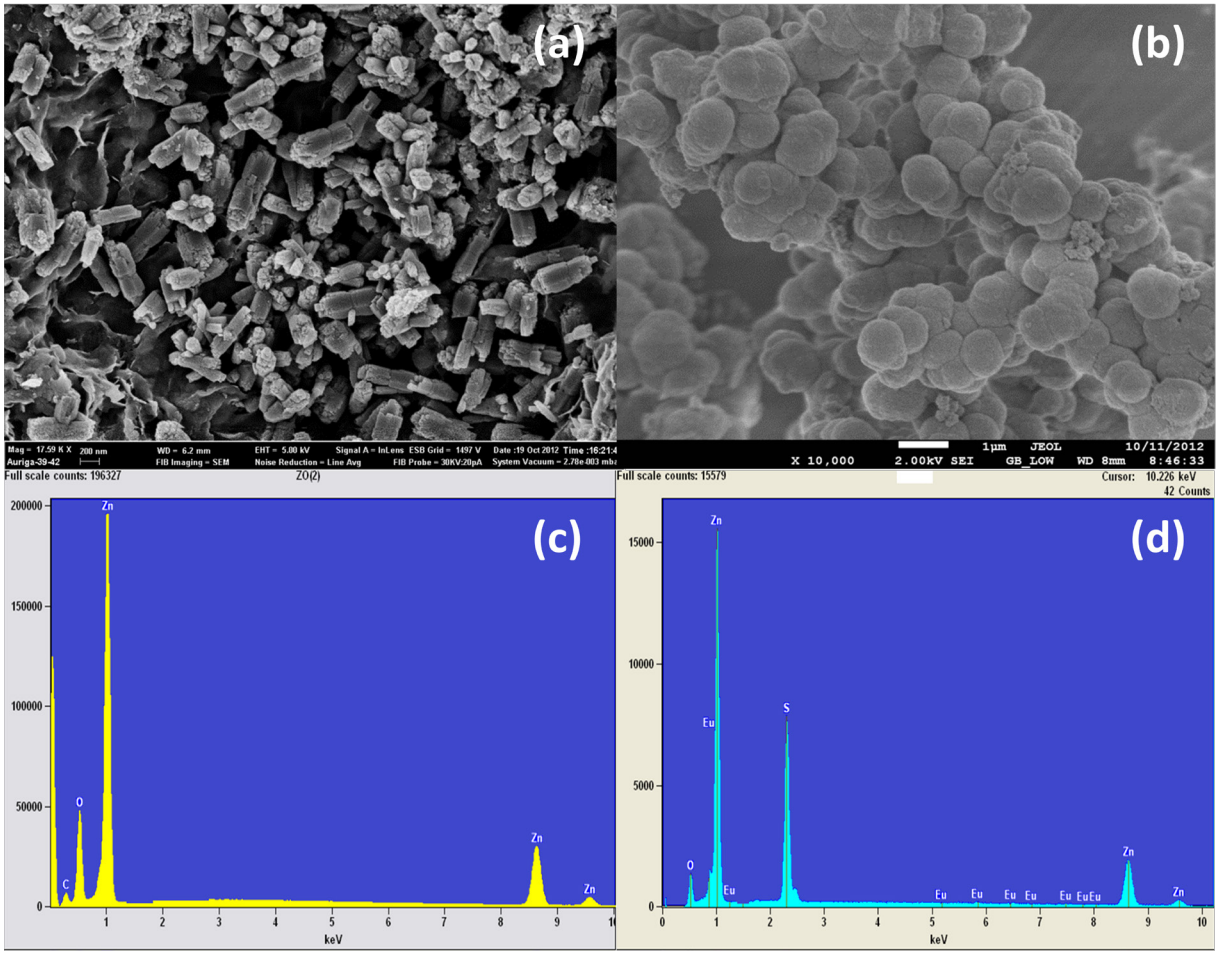

Figure 5. (a) SEM image of ZnO nanorods, (b) SEM image of Eu^{3+}: ZnS spherical nanoparticles, (c) EDS spectrum of ZnO nanorods and (5d) EDS spectrum of Eu^{3+}: ZnS spherical nanoparticles

3.3. UV-Visible Spectroscopy Analysis

Figure 6(a) shows the electronic absorption spectra of ZnO nanorods and Eu^{3+}: ZnS spherical nanoparticles. The absorption band edge recorded for ZnO nanorods and Eu^{3+}: ZnS spherical nanoparticles are 277nm and 300nm, respectively. The band gap energies of the samples were estimated from the Tauc's relation for a direct transition semiconductor[27]:

$$\alpha(\nu) = \frac{(h\nu - E_g)^{1/2}}{h\nu} \tag{16}$$

where the $h\nu$ and E_g is the energy band gap of sample and of the corresponding bulk, respectively and the absorption coefficient $\alpha(\nu)$ can be expressed as[28]:

$$\alpha(\nu) = \left[\frac{1}{d}\ln\left(\frac{1}{T_N}\right)\right] \tag{17}$$

where d is the thickness of sample holder (cuvette) and T_N is the normalized transmittance.

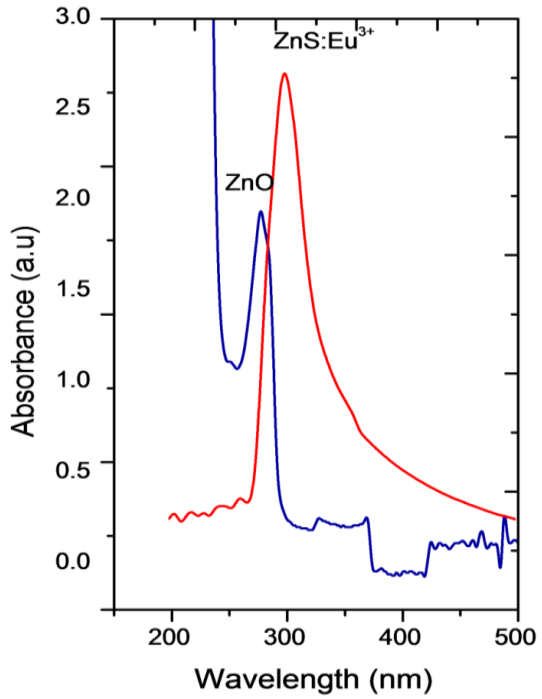

Figure 6a. Absorption spectra of ZnO nanorods and Eu^{3+}: ZnS spherical nanoparticles

The plot of $(\alpha h\nu)^2$ versus $h\nu$ in Fig. 6(b) gives a discontinuity at the absorption band edge of semiconductor nanoparticle. In Fig. 6(b), the intercept at the point of discontinuity on the $h\nu$ axis corresponds to the absorption band edge and it was found to be 4.48 eV and 4.14 eV for ZnO nanorods and Eu^{3+}: ZnS spherical nanoparticles, respectively. Both absorption peaks show considerable blue shift from their bulk values 3.72 eV (cubic zinc blende ZnS) and 3.4 eV (ZnO)], which is a consequence of quantum size effect[29]. It can also be noticed that though ZnO nanorods have larger particle size distribution, its absorption energy is larger than that of Eu^{3+}: ZnS spherical nanoparticles. According to[2], the relative shift of the absorption energy of semiconductors is not exclusively dependent on particle size, but also on the difference between the ionic radius of the dopant and the host cations as well as the chemical nature of the dopants.

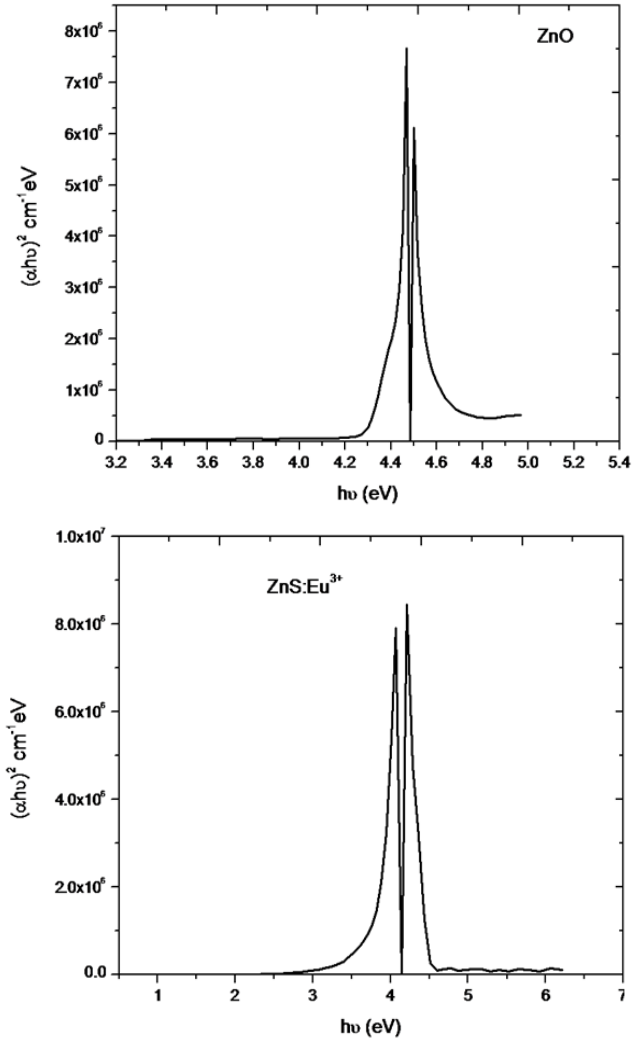

Figure 6b. Energy band gap of ZnO nanorods and Eu^{3+}: ZnS spherical nanoparticles

3.4. Photoluminescence Studies

The results of room temperature photoluminescence emission spectra of ZnO nanorods and Eu^{3+}: ZnS spherical nanoparticles are shown in Fig.7. The emission spectrum of ZnO nanorods shows three prominent shoulders at 413 nm, 441 nm and 586 nm. These peaks become strongest under near-band gap excitation (curve c). The violet emission at 413 nm is assigned to Zn interstitials while the blue emission peak at 441 nm is assigned to direct recombination of conduction electron in the Zn 3d band and a hole in the O_{2P} valence band[30]. The weak green emission peak located at 586 nm is related to the deep-level defect states which is mainly caused by singly ionized oxygen and can be ascribed to the recombination of photogenerated holes with electrons

occupying vacancy and interstitials of zinc[31]. This green emission band (in Fig. 7a) is absent in the ZnS luminescence spectrum (Fig. 7b) suggesting that their formation is solely caused by defects associated with oxygen vacancy. T_N is the normalized transmittance.This result also supports our earlier suggestion that the oxygen in the EDS spectrum may be from air trapped in the SEM chamber.

Luminescence emission in the range 440 nm – 492 nm recorded for Eu^{3+}: ZnS nanoparticles can be ascribed to a self-activated centre formed between a Zn vacancy and a shallow donor associated with sulfur vacancy[17]. It is noted that the interstitially located Zn^{2+} were removed after conversion from ZnO to Eu^{3+}: ZnS. This is evident from the quenching of the violet band located at 413 nm. The removed interstitial Zn^{2+} might have been substituted by S^{2-} which has a larger ionic radius, thus increasing the strain in the ZnS host lattice. Interestingly, the intensity of the blue emission at 440nm remains almost unaltered even after the conversion of ZnO into Eu^{3+}: ZnS, confirming our earlier argument that the blue emission was due to Zn vacancies. The blue-yellow emission band at 520 nm could be formed by the transfer of trapped electrons on the sulfur vacancies to interstitial sulfur states[32]. In addition to the defects related emission bands of ZnS host, transition bands such as $^5D_0 \rightarrow {}^7F_1$ (590 nm – 592 nm), $^5D_0 \rightarrow {}^7F_2$ (614 nm – 629 nm), $^5D_0 \rightarrow {}^7F_5$ (758 nm) and $^5D_0 \rightarrow {}^7F_6$ (882 nm) which are related to Eu^{3+} can also be observed under resonant excitation (Fig. 7(c) and (d)). No such transitions were observed for Eu^{3+}: ZnS spherical nanoparticles under nonresonant excitation at 285 nm demonstrating that no energy transfer from the host ZnS to Eu^{3+} ions using this synthetic procedure, rather transition bands such $^5D_0 \rightarrow {}^7F_5$ and $^5D_0 \rightarrow {}^7F_6$ which are seldom observed were recorded for this sample.

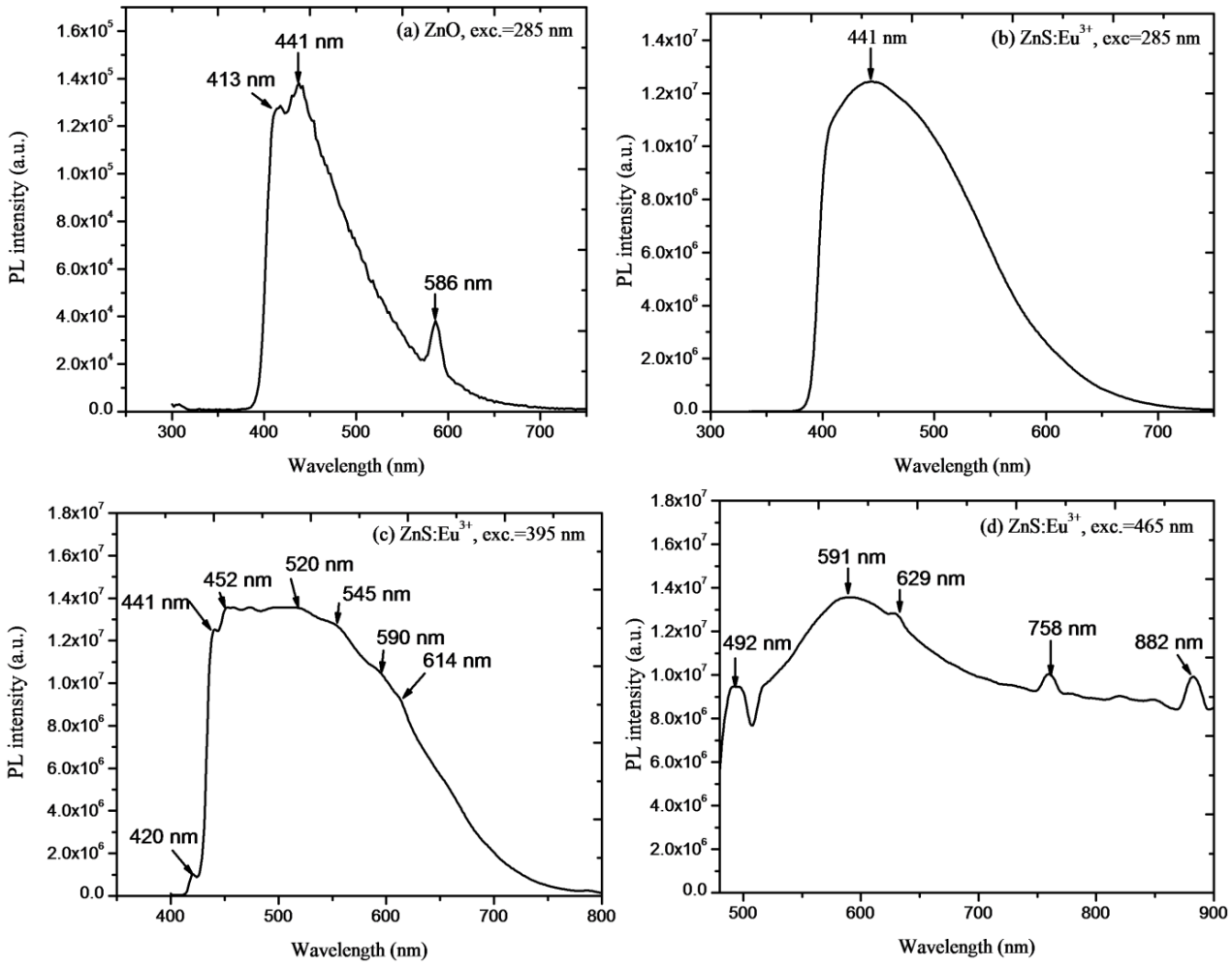

Figure 7. Photoluminescence emission spectra of ZnO nanorods and Eu^{3+}: ZnS spherical nanoparticles

4. Conclusions

Spherical nanoparticles of Eu^{3+}: ZnS semiconductor was synthesized from freshly prepared ZnO nanorod precursor using the precipitation technique. From the XRD patterns, the crystal structures were those of zinc blende and wurzite structures for ZnS and ZnO nanorods, respectively. The Eu^{3+}: ZnS spherical nanoparticles shows considerable strain in their lattice caused by the introduction of Eu^{3+} ion into the ZnS matrix. The difference in ionic size of Eu^{3+} and Zn^{2+} ions could be the reason for the increased lattice distortion. Both defect related emissions as well as dopant (Eu^{3+}) emission bands were observed in the Eu^{3+}-doped ZnS spherical nanoparticles. However, there was no evidence of energy transfer from the host ZnS crystal to the Eu^{3+} ion. For the ZnO nanorod, the photoluminescence emission transitions recorded were solely due to Zn and O related defect sites.

REFERENCES

[1] Binnemans, K., 2009, Lanthanide-based Luminescent hybrid materials. *Chem. Rev.* 109, 4282 – 4374.

[2] Pal M., Pal U., Miguel J., Jimenez G.Y., Perez-Rodriguez F., 2012, Effect of crystallization and dopant concentration on the emission behavior of TiO_2: Eu nanophosphors. *Nanoscale Research Letters*, 7, 1-12.

[3] Banski, M, Podhorodecki, A, Misiewicz, 2010, influence of sol-gel matrices on the optical excitation of emopium ions. *Materials Science – Poland*, 28(1), 217 – 226.

[4] Chen, W; Joly, A.G, Malm, J; Bovin, J., 2004, Up Conversion Luminescence of Eu^{3+} and Mn^{2+} in ZnS: Mn^{2+}, Eu^{3+} codoped nanoparticles. *Journal of Applied Physics, 95, 667 – 672.*

[5] Chowdhurry, P.S., Saha, S. Patra, A., 2004, Influence of nanoenvironment of luminescence of Eu^{3+} activated SnO_2 nanocrystals. *Solid State Communications, 131, 785 – 788.*

[6] Son, C., Kim S., Kim Y., Kim Y.T., Choi I., Wakahara A., Tanoue H. and Ogura M., 2004, Red emission from Eu-Implanted GaN. *Journal of the Korean Physical Society*, 45, S519_S521.

[7] Andrić Z., Dramicanin M.D., Jokanović V., Dramicanin T., Mitrić M. Viana B., 2006, Luminescent properties of nano-SiO_2: Eu^{3+}/polypropylene composite. *Journal Optoelectronics & Advanced Materials*, 8(2), 829-834.

[8] Julian, B., Planelles, J., Cordoncillo, E., Escribano, P., Aschehoug, P., Sanchez, C., Viana, B., Pelle, F., 2006, Eu^{3+} - doped CdS nanocrystals in SiO_2 matrices: one-pot sol-gel synthesis and optical characterization. *Journal of Material Chemistry, 16, 4612- 4618.*

[9] Liu, Y., Luo, W., Li, R., Liu, G., Antonio, M.R., Chen, X., 2008, Optical spectroscopy of Eu^{3+} Doped ZnO Nanocrystals. *J. Phys. Chem. C, 112, 686 – 694.*

[10] Planelles-Aragó, J., Julian – Lopez, B., Cordoncillo, E., Escribano, P., Pelle, F., Viana, B., Sanchez, C., 2008, lanthanide doped ZnS quantum dots dispersed in silica glasses: an easy one pot sol-gel synthesis for obtaining novel photonic materials. *J. Matter. Chem*. 18, 5193 – 5199.

[11] Sun X.L., Zhang, G.l., Tang G.Q., Chen W.J., 1999, Site symmetry of Eu^{3+} in ZnS:Eu nanoparticles. *Chinese Chemical Letters,* 10 (9), 807 – 810.

[12] Qu, S.C. Zhou, W.H., Liu, F.Q., Chen, N.F., Wang, Z.G., 2002, Photoluminescence properties of Eu^{3+} - doped ZnS Nanocrystals prepared in a water/methanol solution. *Applied Physics Letters*, 8(19**)**, 3605 – 3607.

[13] Bol A.A., Van Beek, R, and Meijerink A., 2002, on the incorporation of trivalent rare-earth ions in II – VI Semiconductor Nanocrystals. *Chem. Mater. 14, 1121-1126.*

[14] Rubio M.I., Irland T.G., Fem G.R., Silver J., Snowden M.J., 2001, A new application for microgels: Novel methods for the synthesis of spherical particles of Y_2O_3:Eu phosphor using copolymer microgel of NIPAM and acrylic acid. *Lagmuir*, 147, 7145 – 7149.

[15] Kang Y.C., Park S.B., Lenggoro I.W., Okuyama K., 1999, Gd_2O_3:Eu phosphor particles with sphericity, submicron size and non-aggregation characteristics. *Journal of Physics & Chemistry of Solids*, 60, 379 – 384.

[16] Jia P.Y., Liu X.M., Yu M., Luo Y., Fang J., Lin J., 2006, Luminescence properties of sol-gel derived spherical $SiO_2@Gd_2(WO_4)_3$: Eu^{3+} particles with core-shell structure. *Chemical Physics Letters*, 424, 358 – 363.

[17] Liu J.Z., Yan P.X., Yue G.H., Chang J.B., Qu D.M. and Zhuo R.F., 2006, Red light photoluminescence emission from Mn and Cd co-doped ZnS one-dimensional nanostructures. *Journal of Physics D. Applied Physics*, 39, 2352 – 2356.

[18] Rhehani B.R., Joshi P.B., Kirit N.L. and Pratap A., 2006, Crystalline size estimation of elemental and composite silver nano-powders using XRD principles. *Indian Journal of Pure & Applied Physics*, 44, 157-161.

[19] Reddy B.K., 2010, Investigation of ZnS nanoparticles based on synthesis temperature for optoelectronic device application. *Journal of Optoelectronics & Advanced Materials,* 12(11), 2185 – 2189.

[20] Mazhdi M. & Khani P.H., 2013, Structural characterization of ZnO and ZnO:Mn nanoparticles prepared by reverse micelle method. *Int. J. Nano. Dim*. 2(4), 233 – 240.

[21] Gu F., Wang S.F., Lu M.K., Zhou G.J., Xu D. and Yuan D.R., 2004, Structure Evaluation and Highly Enhanced Luminescence of Dy^{3+} - Doped ZnO Nanocrystals by Li^+ Doping via combustion method. *Langmuir* 20, 3528 – 3531.

[22] Wongsaprom K. and Maensiri S., 2013, Synthesis and Room Temperature Magnetic Behaviour of Nickel Oxide Nanocrystallites. *Chiang Mai J. Sci.* 40(1), 99 - 108.

[23] Bueno-Ferrer C., Pares-Eschapez S., Lozano-Castello D., Bueno-Lopez A., 2010, Relationship between surface area and crystal size of pure and doped cerium oxides. *Journal of Rare-earth,* 28(5), 647.

[24] Gschneidner K.A., Bunzli C.G. and Pecharsky V.K., 2007, Handbook on the Physics and Chemistry of Rare Earths: Optical Spectroscopy, 37, North-Holland Elsevier B.V., Amsterdam.

[25] Mehta, S.K, Kumar, S., Chaudhary, S., Bhasin, K.K., 2009, Effect of cationic surfactant Head Groups on Synthesis,

Growth and Agglomeration Behaviour of ZnS Nanoparticles. *Nanoscale Rev. Lett. 4, 1197 – 1208.*

[26] Yi R., Qu G., Liu X., 2009, Rational synthetic strategy: From ZnO nanorods to ZnS nanotubes. *Journal of Solid Chemistry*, 182, 2791 – 2795.

[27] Kilic G. and Aral E., 2009, Determination of optical band gaps and structural properties of Cu^{2+} doped B_2O_3-Na_2O – Al_2O_3- V_2O_2. *G.U.Journal of Science* 22(3), 129 -139.

[28] Ahemen I., Meludu O. and Odoh E., 2013, Effect of Sodium Carboxymethyl Cellulose Concentration on the Photophysical Properties of Zinc Sulfide Nanoparticles. *British Journal of Applied Science and Technology*, 3(4), 1228-1245.

[29] Fang X., Zhai T., Gautam U.K., Li L., Wu L., Bando Y. and Golberg D., 2011, ZnS nanostructures: From synthesis to applications. *Progress in Materials Science*, 56, 175-287.

[30] Kundu T.K., Karak N., Barik P., Saha S., 2011, Optical properties of ZnO nanoparticles prepared by chemical method using Poly (Vinyl Alcohol) (PVA) as capping agent. *International Journal of Soft Computing & Engineering (IJSCE)*, 1, 19-24.

[31] Dutta S. and Ganguly B.N., 2012, Characterization of ZnO nanoparticles grown in presence of folic acid template. *Journal of Nanotechnology*, 10(29), 1-10.

[32] Wang X., Shi J., Feng Z., Li M., Li C., 2011, Visible emission characteristics from different defects of ZnS nanocrystals. *Phys. Chem. Chem. Phys*., 13, 4715-4723.